



# Hyperspectral Sparse Unmixing With Spectral-Spatial Low-Rank Constraint

Fan Li, Shaoquan Zhang , *Member, IEEE*, Bingkun Liang, Chengzhi Deng , Chenguang Xu, and Shengqian Wang

**Abstract**—Spectral unmixing is a consequential preprocessing task in hyperspectral image interpretation. With the help of large spectral libraries, unmixing is equivalent to finding the optimal subset of the library entries that can best model the image. Sparse regression techniques have been widely used to solve this optimization problem, since the number of materials present in a scene is usually small. However, the high mutual coherence of library signatures negatively affects the sparse unmixing performance. To cope with this challenge, a new algorithm called spectral-spatial low-rank sparse unmixing (SSLRSU) is established. In this article, the double weighting factors under the  $\ell_1$  framework aim to improve the row sparsity of the abundance matrix and the sparsity of each abundance map. Meanwhile, the low-rank regularization term exploits the low-dimensional structure of the image, which makes for accurate endmember identification from the spectral library. The underlying optimization problem can be solved by the alternating direction method of multipliers efficiently. The experimental results, conducted by using both synthetic and real hyperspectral data, uncover that the proposed SSLRSU strategy can get accurate unmixing results over those given by other advanced sparse unmixing strategies.

**Index Terms**—Hyperspectral imaging, low-rank constraint, sparse unmixing, weighted sparse regression.

## I. INTRODUCTION

**H**YPERSPECTRAL imaging collects hundreds of images, using different wavelength channels, for the same area on the surface of the Earth [1]. Therefore, it is possible to realize quantitative and refined Earth observation research [2]. At present, hyperspectral remote sensing technologies have been widely used in mineral exploration, environmental monitoring,

military applications, etc [3]. However, limited by the spatial resolution of imaging spectrometers and the complexity of ground features, there are a large number of mixed pixels in hyperspectral images [4], which greatly hinders the further exploration of the hyperspectral image information. Spectral unmixing is an effective way for the mixing problem, which estimates the pure spectral endmembers and their corresponding fractional abundances in each mixed pixel [5].

For the past years, linear mixture model-based approaches have been widely studied in the field of hyperspectral unmixing, such as minimum volume algorithms [6]–[8] and nonnegative matrix factorization (NMF)-based algorithms [9]–[11] achieve remarkable performance, among which sparse unmixing [12] relying on spectral libraries becomes one of the most active research topics. The purpose of sparse unmixing is to find the optimal subset of entries in a large spectral library which can best model the mixed pixels in the hyperspectral image. In the beginning, some sparse unmixing methods focused on the exploration of the sparse characteristic from the spectral viewpoint. For instance, the sparse unmixing algorithm via variable splitting and augmented Lagrangian (SUNSAL) [12] adopts the  $\ell_1$  regularizer to measure the sparsity on the abundance matrix. The  $\ell_p$  (for  $0 \leq p < 1$ ) regularizer [13] and other nonconvex approximations [14] are used to further impose sparsity. The collaborative SUNSAL (CLSUNSAL) [15] algorithm introduces the  $\ell_{2,1}$  regularizer to impose the global row sparsity of the matrix. Furthermore, the double reweighted sparse unmixing (DRSU) [16] algorithm introduces the double weighting factors to penalize nonzero coefficients in the solution, and obtains promising results.

Recently, in order to promote the spatial correlation of images, a new trend is to incorporate spatial information into the sparse unmixing models [17], [18]. For example, the well-known total variation (TV) spatial regularization [19], [20] is used to promote the smoothness of abundance maps. The superpixel segmentation technology [21]–[23] is employed to design adaptive neighborhoods with more accurate spatial-contextual information. The nonlocal similarity [24] is adopted to preserve the nonlocal spatial structure on abundance maps. Furthermore, the spectral and spatial weighting factors [25] are introduced into the  $\ell_1$  unmixing framework to consolidate the spatial connection.

The high spatial correlation of the image implies the low rankness of the abundance matrix [26]. Accordingly, when the low-rank constraint is imposed on the abundance matrix, the low-dimensional subspace structure of the image will be well preserved [27]. More recently, the sparsity and low-rank

Manuscript received March 23, 2021; revised May 9, 2021; accepted May 21, 2021. Date of publication June 4, 2021; date of current version June 28, 2021. This work was supported in part by National Natural Science Foundation of China under Grant 61901208 and Grant 61865012, in part by China Postdoctoral Science Foundation under Grant 2020M672483, in part by the Science and Technology Project of Jiangxi Provincial Department of Education under Grant GJJ190956 and Grant GJJ170992, in part by Basic Science and Technology Research Project of National Key Laboratory of Science and Technology on Automatic Target Recognition under Grant WDZC20205500204, and in part by Jiangxi Provincial Key Research and Development Program under Grant 20202BBGL73081 and Grant 20181ACG70022. (Corresponding author: Shaoquan Zhang and Chengzhi Deng.)

Fan Li, Shaoquan Zhang, Chengzhi Deng, Chenguang Xu, and Shengqian Wang are with the Jiangxi Province Key Laboratory of Water Information Cooperative Sensing, and Intelligent Processing, School of Information Engineering, Nanchang Institute of Technology, Nanchang 330099, China (e-mail: lifan@nit.edu.cn; zhangshaoquan1@163.com; dengcz@nit.edu.cn; xcg@nit.edu.cn; sqwang113@263.net).

Bingkun Liang is with the Guangdong Provincial Key Laboratory of Urbanization, and Geo-simulation, School of Geography and Planning, Sun Yat-sen University, Guangzhou 510275, China (e-mail: liangbk@mail2.sysu.edu.cn).

Digital Object Identifier 10.1109/JSTARS.2021.3086631

constraints [28] were simultaneously imposed on the abundance matrix to reduce the solution space. In [29], a subspace unmixing with low-rank attribute embedding method was proposed to alleviate the influence of spectral variability on the unmixing results. In [30], the abundance matrix is converted to 3D, and the low-rank properties are exploited by using local blocks. In [31], the joint-sparse-blocks and low-rank unmixing (JSpBLRU) algorithm was developed to enhance the sparsity along the rows within each block, and the desired results were obtained.

The aforementioned spectral unmixing approaches with the dual constraints have achieved remarkable performance. It is well known that pixels with the same or similar components and proportions are highly correlated, thus the abundance vectors corresponding to the ones are dependent. Reduced-rank abundance matrix uncovers the spatial low-dimensional structure and enhances the spatial correlation of the image. The joint constraint of low-rank and sparsity aims to obtain a low-rank approximation of the sparse solution. The unmixing technique with the aforementioned constraints makes for weakening the interference of other similar spectral signatures in the library, and finding the actual spectral signatures in the scene from the library more accurately. However, the above methods still have some shortcomings in endmember identification. It is a challenging problem to deal with the high mutual coherence of spectral libraries.

In order to better handle the high mutual coherence between spectral signatures in the library as well as consider the low-rank spatial structure of the abundance, a new spectral-spatial low-rank sparse unmixing (SSLRSU) is proposed. In this article, the double weighting factors under the  $\ell_1$  framework are used to improve the sparsity of the abundance matrix. Meanwhile, the low-rank constraint exploits the low-dimensional structure of the image and accurately identify endmember signatures from the spectral library. In terms of its computational complexity, the proposed SSLRSU can be efficiently solved by the notable alternating direction method of multipliers (ADMM) [32].

The main contributions of our work can be summarized as follows.

- 1) For our new SSLRSU algorithm, the double weighting factors are utilized to upgrade the sparsity of the arrangement, while the low-rank constraint is used to preserve the spatial low-dimensional structure of abundance maps and improve the ability to identify endmembers from the spectral library. The spectral-spatial low-rank constraint effectively alleviates the negative impact of the high mutual coherence of the spectral library on the unmixing results.
- 2) In terms of iterative optimization, the proposed SSLRSU model is iteratively solved by an inner and outer loop scheme, where the inner loop updates the Lagrange multipliers by ADMM, and the outer loop updates the double weights. It can speed up the convergence of the algorithm.

The rest of this article is organized as follows. The proposed SSLRSU unmixing technique (and its solution algorithm) are described in detail in Section II. Sections III and IV portray the experimental results with simulated and real hyperspectral datasets. Finally, Section V concludes this article.

## II. PROPOSED SPECTRAL-SPATIAL LOW-RANK SPARSE UNMIXING ALGORITHM

### A. Sparse Unmixing

Sparse unmixing solves the linear spectral mixture problem in dictionary-based semisupervised fashion. It assumes that the observed hyperspectral image can be expressed as a linear combination of certain spectral signatures known in advance. Therefore, the spectral library is introduced to approach the unmixing problem instead of extracting or generating endmembers from the original hyperspectral image. Unmixing is equivalent to finding the optimal subset of spectral signatures in the library that can best model images. Let  $\mathbf{Y} \in \mathbb{R}^{d \times n}$  be a hyperspectral image, where  $d$  and  $n$  are the numbers of bands and pixels, respectively. The sparse unmixing model can be written as follows:

$$\mathbf{Y} = \mathbf{A}\mathbf{X} + \mathbf{N} \quad (1)$$

where  $\mathbf{A} \in \mathbb{R}^{d \times m}$  denotes the spectral library containing  $m$  spectral signatures,  $\mathbf{X} \in \mathbb{R}^{m \times n}$  denotes the abundance matrix with regard to the library  $\mathbf{A}$ , and  $\mathbf{N} \in \mathbb{R}^{d \times n}$  denotes the noise or model error.

The abundance matrix indicates the proportion of each endmember in the spectral library participating in mixed pixels. Since each mixed pixel consists of only a few endmembers compared with the large spectral library, the abundance matrix usually contains a lot of zero values, that is,  $\mathbf{X}$  is sparse. According to this analysis, sparse unmixing can be reformulated as an  $\ell_2$ - $\ell_0$ -norm optimization problem as follows:

$$\min_{\mathbf{X}} \frac{1}{2} \|\mathbf{Y} - \mathbf{A}\mathbf{X}\|_F^2 + \lambda \|\mathbf{X}\|_0 \quad \text{s.t. } \mathbf{X} \geq 0 \quad (2)$$

where  $\|\cdot\|_F$  is the Frobenius norm,  $\lambda \geq 0$  is a regularization parameter that tradeoff the sparsity regularization term and the data fitting term,  $\|\mathbf{X}\|_0$  denotes the number of nonzero values of  $\mathbf{X}$ , and  $\mathbf{X} \geq 0$  is a physical constraint called abundance nonnegativity constraint (ANC). Notice that another physical constraint called abundance sum-to-one constraint (ASC) is not imposed on the  $\mathbf{X}$  due to the drawbacks mentioned in [12]. The  $\ell_0$ -norm in (2) leads to an NP-hard problem, which can be relaxed to  $\ell_1$ -norm under the condition of restricted isometric property (RIP) [33], [34]. The optimization problem (2) is replaced as follows:

$$\min_{\mathbf{X}} \frac{1}{2} \|\mathbf{Y} - \mathbf{A}\mathbf{X}\|_F^2 + \lambda \|\mathbf{X}\|_{1,1} \quad \text{s.t. } \mathbf{X} \geq 0 \quad (3)$$

where  $\|\mathbf{X}\|_{1,1} = \sum_{j=1}^n \|\mathbf{x}_j\|_1$ ,  $\mathbf{x}_j$  is the  $j$ th column vector of  $\mathbf{X}$ .

The problem (3) has been solved by the SUnSAL algorithm [32]. Nevertheless, the  $\ell_1$ -norm minimization problem is subject to a few inherent shortcomings: 1) It focuses on analyzing the abundance vector of each single pixel without exploiting spatial structure information for abundance estimation. 2) The sparsity of real abundance maps is generally beyond the reach of the  $\ell_1$ -norm. 3) As an underdetermined system of equations, its uniqueness of the sparsest solution is severely limited by the high mutual coherence of the spectral library. The mutual coherence

of the spectral library  $\mathbf{A}$  is given by

$$\mu(\mathbf{A}) = \max_{1 \leq k, j \leq m, k \neq j} \frac{|\mathbf{a}_k^T \mathbf{a}_j|}{\|\mathbf{a}_k\|_2 \|\mathbf{a}_j\|_2} \quad (4)$$

where  $\|\cdot\|_2$  is the  $\ell_2$ -norm,  $\mathbf{a}_k$  is the  $k$ th column vector of  $\mathbf{A}$ . Mutual coherence computes the maximum cosine angle distance between any different columns in the system matrix, whose value lies in the range  $[0, 1]$ . The coherence characterizes the dependence between the columns of the matrix. Unfortunately, the mutual coherence of the spectral library is close to one, which indicates that the spectral signatures in the library are very similar [35]. The highly correlated spectral signatures have a negative impact on the uniqueness of the solution, and multiple solutions for abundance estimation imply the uncertainty of endmembers identification [36]. Specifically, the single endmember may be interpreted as multiple similar spectral signatures or incorrect spectral signature [37], [38]. The high sparsity of the abundance vector balances this undesired aspect, and the reduction of nonzero rows in the abundance matrix facilitates the search for the optimal subset of signatures in the library [39].

### B. Proposed SSLRSU Model

The sparsity constraint plays an important role in improving the performance of sparse unmixing. A sufficiently sparse solution means a precise abundance estimation. It has been found that the reweighted  $\ell_1$ -norm can effectively and flexibly enhance the sparsity of the solution [16], [20], [25], [40]. Moreover, low-rankness is another intrinsic structural feature of the abundance matrix [28], which motivates the integration of low-rank constraint into the sparse unmixing model. Inspired by the above ideas, the SSLRSU model is proposed, as follows:

$$\begin{aligned} \min_{\mathbf{X}} \quad & \frac{1}{2} \|\mathbf{Y} - \mathbf{A}\mathbf{X}\|_F^2 + \lambda \|(\mathbf{H}_1 \mathbf{H}_2) \odot \mathbf{X}\|_{1,1} \\ & + \tau \text{rank}(\mathbf{X}) \text{ s.t. } \mathbf{X} \geq 0. \end{aligned} \quad (5)$$

The double weighting factors are incorporated into the  $\ell_1$ -norm, which offsets the imperfect measurement of the sparsity of fractional abundances in the original method to a certain extent. The weighting factor  $\mathbf{H}_1$  aims to enhance the row sparsity of the abundance matrix. It can be construed as selecting fewer spectral signatures (endmembers) from the spectral library to model the image.  $\mathbf{H}_1 \in \mathbb{R}^{m \times m}$  is an iterative diagonal matrix, defined as

$$\mathbf{H}_1^{(t+1)} = \text{diag} \left[ \frac{1}{\|\mathbf{X}^{(t)}(1, :)\|_2 + \varepsilon}, \dots, \frac{1}{\|\mathbf{X}^{(t)}(i, :)\|_2 + \varepsilon} \right] \quad (6)$$

where  $\mathbf{X}^{(t)}(i, :)$  is the  $i$ th row of  $\mathbf{X}$  at the  $t$ th iteration and  $\varepsilon > 0$  is a small constant added to avoid singularities. Each entry in  $\mathbf{H}_1$  is inversely proportional with the  $\ell_2$ -norm value of the corresponding row vector in the abundance matrix. Guided by the weights, the nonzero rows of estimated abundances will be concentrated to the rows with larger values in each iteration. The weighting factor  $\mathbf{H}_1$  enforces the row sparsity of the abundance matrix in a natural way. That is to say, there will be fewer endmembers taking part in the expression of the image, thereby removing part of the highly correlated spectral signatures limitations. The other weighting factor  $\mathbf{H}_2 \in \mathbb{R}^{m \times n}$  is introduced to improve the

sparsity of the solution, defined as

$$\mathbf{H}_2^{(t+1)}(i, j) = \frac{1}{\mathbf{X}^{(t)}(i, j) + \varepsilon} \quad (7)$$

where  $\mathbf{H}_2^{(t+1)}(i, j)$  denotes the  $i$ th row and  $j$ th column element in  $\mathbf{H}_2$  at the  $(t+1)$ th iteration and  $\mathbf{X}^{(t)}(i, j)$  denotes the  $i$ th row and  $j$ th column element in  $\mathbf{X}$  at the  $t$ th iteration. The weighting factor  $\mathbf{H}_2$  encourages the larger fractional abundance by smaller weight values iteratively and vice versa. It more efficiently reduces the nonzero elements contained in fractional abundances. The operator  $\odot$  denotes the Hadamard product of two variables. The sparsity-inducing regularizer in the form of double weighted  $\ell_1$ -norm can not only obtain more sparse solutions but also model the image with fewer endmembers.

The low-rank regularization term captures the spatial structure of hyperspectral data by seeking the lowest rank representation of the abundance matrix. More precisely, abundance vectors can be considered to be linearly dependent due to the spatial correlation of pixels in a scene. Therefore, besides the traditional sparse constraints, the low-rank regularizer is also employed to reduce the solution space in abundance estimation. It is well known that matrix rank minimization is an NP-hard problem. Nuclear norm minimization, as a relaxation to the low-rank regularizer, is a common alternative to directly calculating the rank of the matrix [41], [42]. The rank of  $\mathbf{X}$  is replaced by its nuclear norm, the problem (5) is represented as follows:

$$\begin{aligned} \min_{\mathbf{X}} \quad & \frac{1}{2} \|\mathbf{Y} - \mathbf{A}\mathbf{X}\|_F^2 + \lambda \|(\mathbf{H}_1 \mathbf{H}_2) \odot \mathbf{X}\|_{1,1} \\ & + \tau \|\mathbf{X}\|_* \text{ s.t. } \mathbf{X} \geq 0 \end{aligned} \quad (8)$$

where  $\|\mathbf{X}\|_* = \sum_{i=1}^r \sigma_i(\mathbf{X})$ ,  $\sigma_i(\mathbf{X})$  denotes the  $i$ th singular value of  $\mathbf{X}$  and  $r = \text{rank}(\mathbf{X})$ .

Nuclear norm can be easily solved by existing convex optimization tools. But they treat all singular values equally, which will lead to a bias to the matrix with small singular values. The weighted nuclear norm minimization (WNNM) mitigates the punishment bias between larger singular values and small singular values by assigning smaller weights to larger values and larger weights to smaller values [43]. The iteratively weighted nuclear norm of  $\mathbf{X}$  is defined as

$$\|\mathbf{X}\|_{b,*}^{(t+1)} = \sum_{i=1}^r b_i^{(t)} \sigma_i^{(t)}(\mathbf{X}) \quad (9)$$

where  $b_i^{(t)} = \frac{1}{\sigma_i^{(t)}(\mathbf{X}) + \varepsilon}$ ,  $\varepsilon > 0$  is a small constant added to avoid singularities. It is known that larger singular values generally retain the main information of the matrix. The WNNM mitigates the punishment on larger singular values of  $\mathbf{X}$ , so the corresponding shrinkage is small and most of information is well preserved. Meanwhile, the WNNM takes serious shrinkage on smaller singular values, thereby generating a lot of zero singular values, leaving only several largest singular values of  $\mathbf{X}$ . The low-dimensional approximation of  $\mathbf{X}$  is obtained after a series of weighted singular value shrinkages. Rank measures the second-order sparsity of a matrix, since it is closely related to the correlation among columns and rows of the matrix [44]. On the one hand, the low-rank abundance matrix captures the

correlation of pixels, which encourages mixed pixels to share the same endmembers and similar abundance maps. On the other hand, it promotes the reduction of linearly independent vectors in the abundance matrix while ensuring that the main information of fractional abundances can be preserved. In the case that the double weighting factors promote the row sparsity of the abundance matrix, the reduced-rank matrix helps to determine the endmembers accurately, and removes part of mismatches caused by the highly similar spectral signatures.

Finally, the SSLRSU model is represented as

$$\begin{aligned} \min_{\mathbf{X}} \quad & \frac{1}{2} \|\mathbf{Y} - \mathbf{A}\mathbf{X}\|_F^2 + \lambda \|(\mathbf{H}_1\mathbf{H}_2) \odot \mathbf{X}\|_{1,1} + \tau \|\mathbf{X}\|_{b,*} \\ \text{s.t.} \quad & \mathbf{X} \geq 0. \end{aligned} \quad (10)$$

The proposed SSLRSU model simultaneously explores the spectral dual sparsity as well as the spatial low-dimensional structural information of fractional abundances. By reducing the number of spectral signatures participating in expressing hyperspectral data and searching for exact match between the actual spectral signatures in the image and the samples in the spectral library, the proposed model can cope with the negative influence of the high coherence of the spectral library on the unmixing results.

### C. Solution of the Optimization Problem

In this section, we use the alternating direction method of multipliers (ADMM) to solve the SSLRSU model in (10). Utilizing five auxiliary matrix variables  $\mathbf{U}$ ,  $\mathbf{V}_1$ ,  $\mathbf{V}_2$ ,  $\mathbf{V}_3$ ,  $\mathbf{V}_4$ , we reformulate the original problem (10) into an equivalent form as

$$\begin{aligned} \min_{\mathbf{U}, \mathbf{V}_1, \mathbf{V}_2, \mathbf{V}_3, \mathbf{V}_4} \quad & \frac{1}{2} \|\mathbf{Y} - \mathbf{V}_1\|_F^2 + \lambda \|(\mathbf{H}_1\mathbf{H}_2) \odot \mathbf{V}_2\|_{1,1} \\ & + \tau \|\mathbf{V}_3\|_{b,*} + \iota_{R+}(\mathbf{V}_4) \\ \text{s.t.} \quad & \mathbf{V}_1 = \mathbf{A}\mathbf{U}, \mathbf{V}_2 = \mathbf{U}, \mathbf{V}_3 = \mathbf{U}, \mathbf{V}_4 = \mathbf{U} \end{aligned} \quad (11)$$

where  $\mathbf{U} = \mathbf{X}$ , and  $\iota_{R+}(\mathbf{X}) = \sum_{i=1}^n \iota_{R+}(\mathbf{x}_i)$  is the indicator function, i.e.,  $\iota_{R+}(\mathbf{x}_i)$  is zero if  $\mathbf{x}_i$  belongs to the nonnegative orthant and  $+\infty$  otherwise.

To make notations more concise, we rewrite (11) in a compact form

$$\min_{\mathbf{U}, \mathbf{V}} g(\mathbf{U}, \mathbf{V}) \quad \text{s.t.} \quad \mathbf{G}\mathbf{U} + \mathbf{B}\mathbf{V} = \mathbf{0} \quad (12)$$

where  $g(\mathbf{U}, \mathbf{V}) = \frac{1}{2} \|\mathbf{Y} - \mathbf{V}_1\|_F^2 + \lambda \|(\mathbf{H}_1\mathbf{H}_2) \odot \mathbf{V}_2\|_{1,1} + \tau \|\mathbf{V}_3\|_{b,*} + \iota_{R+}(\mathbf{V}_4)$ ,  $\mathbf{G} = (\mathbf{A}, \mathbf{I}, \mathbf{I}, \mathbf{I})^T$ ,  $\mathbf{B} = \text{diag}(-\mathbf{I})$ ,  $\mathbf{V} = (\mathbf{V}_1, \mathbf{V}_2, \mathbf{V}_3, \mathbf{V}_4)^T$ . By introducing the scaled Lagrange multipliers  $\mathbf{D} = (\mathbf{D}_1, \mathbf{D}_2, \mathbf{D}_3, \mathbf{D}_4)^T$ , the augmented Lagrangian for (12) is written as

$$\mathcal{L}(\mathbf{U}, \mathbf{V}, \mathbf{D}) = g(\mathbf{U}, \mathbf{V}) + \frac{\mu}{2} \|\mathbf{G}\mathbf{U} + \mathbf{B}\mathbf{V} - \mathbf{D}\|_F^2 \quad (13)$$

where  $\mu > 0$  is a penalty parameter. Now, we implement the ADMM to solve the optimization problem (12), by minimizing  $\mathcal{L}(\mathbf{U}, \mathbf{V}, \mathbf{D})$  with respect to  $\mathbf{U}$  and  $\mathbf{V}$  sequentially and updating

D. Thus, we get:

$$\begin{cases} \mathbf{U}^{(k+1)} = \arg \min_{\mathbf{U}} \mathcal{L}(\mathbf{U}, \mathbf{V}^{(k)}, \mathbf{D}^{(k)}) \\ \mathbf{V}^{(k+1)} = \arg \min_{\mathbf{V}} \mathcal{L}(\mathbf{U}^{(k+1)}, \mathbf{V}, \mathbf{D}^{(k)}) \\ \mathbf{D}^{(k+1)} = \mathbf{D}^{(k)} - (\mathbf{G}\mathbf{U}^{(k+1)} + \mathbf{B}\mathbf{V}^{(k+1)}). \end{cases} \quad (14)$$

The subproblems of  $\mathbf{U}$  and  $\mathbf{V}$  in (14) have closed form solutions. The  $\mathbf{U}$ -subproblem is a least-squares problem as follows:

$$\begin{aligned} \mathbf{U}^{(k+1)} = \arg \min_{\mathbf{U}} \quad & \frac{\mu}{2} \|\mathbf{A}\mathbf{U} - \mathbf{V}_1^{(k)} - \mathbf{D}_1^{(k)}\|_F^2 + \\ & + \frac{\mu}{2} \|\mathbf{U} - \mathbf{V}_2^{(k)} - \mathbf{D}_2^{(k)}\|_F^2 \\ & + \frac{\mu}{2} \|\mathbf{U} - \mathbf{V}_3^{(k)} - \mathbf{D}_3^{(k)}\|_F^2 \\ & + \frac{\mu}{2} \|\mathbf{U} - \mathbf{V}_4^{(k)} - \mathbf{D}_4^{(k)}\|_F^2. \end{aligned} \quad (15)$$

The solution of (15) is

$$\begin{aligned} \mathbf{U}^{(k+1)} = & (\mathbf{A}^T \mathbf{A} + 3\mathbf{I})^{-1} (\mathbf{A}^T (\mathbf{V}_1^{(k)} + \mathbf{D}_1^{(k)}) \\ & + \mathbf{V}_2^{(k)} + \mathbf{D}_2^{(k)} + \mathbf{V}_3^{(k)} + \mathbf{D}_3^{(k)} + \mathbf{V}_4^{(k)} + \mathbf{D}_4^{(k)}). \end{aligned} \quad (16)$$

The  $\mathbf{V}$ -subproblem of (14) is decomposed into four independent subparts related to  $\mathbf{V}_1$ ,  $\mathbf{V}_2$ ,  $\mathbf{V}_3$ ,  $\mathbf{V}_4$ . The optimized solution for  $\mathbf{V}_1$  is calculated as follows:

$$\begin{aligned} \mathbf{V}_1^{(k+1)} = \arg \min_{\mathbf{V}_1} \quad & \frac{1}{2} \|\mathbf{Y} - \mathbf{V}_1\|_F^2 \\ & + \frac{\mu}{2} \|\mathbf{A}\mathbf{U}^{(k+1)} - \mathbf{V}_1 - \mathbf{D}_1^{(k)}\|_F^2 \\ = \frac{1}{1 + \mu} & [\mathbf{Y} + \mu(\mathbf{A}\mathbf{U}^{(k+1)} - \mathbf{D}_1^{(k)})]. \end{aligned} \quad (17)$$

In the same vein, we get the least-squares problem regarding  $\mathbf{V}_2$  as follows:

$$\begin{aligned} \mathbf{V}_2^{(k+1)} = \arg \min_{\mathbf{V}_2} \quad & \lambda \|(\mathbf{H}_1\mathbf{H}_2) \odot \mathbf{V}_2\|_{1,1} \\ & + \frac{\mu}{2} \|\mathbf{U}^{(k+1)} - \mathbf{V}_2 - \mathbf{D}_2^{(k)}\|_F^2. \end{aligned} \quad (18)$$

Since problem (18) is componentwise separable, the solution of  $\mathbf{V}_2$  is

$$\mathbf{V}_2^{(k+1)} = \text{soft}(\mathbf{U}^{(k+1)} - \mathbf{D}_2^{(k)}, \frac{\lambda}{\mu} \mathbf{H}_1\mathbf{H}_2) \quad (19)$$

where  $\text{soft}(\cdot, \cdot)$  is a soft-threshold function defined by  $\text{soft}(y, \tau) = \text{sign}(y) \max\{|y| - \tau, 0\}$ .

The subproblem regarding  $\mathbf{V}_3$  can be solved by a shrinkage operation as follows:

$$\begin{aligned} \mathbf{V}_3^{(k+1)} = \arg \min_{\mathbf{V}_3} \quad & \tau \|\mathbf{V}_3\|_{b,*} + \frac{\mu}{2} \|\mathbf{U}^{(k+1)} - \mathbf{V}_3 - \mathbf{D}_3^{(k)}\|_F^2 \\ = \text{SVT}_{b, \frac{\tau}{\mu}} & (\mathbf{U}^{(k+1)} - \mathbf{D}_3^{(k)}) \end{aligned} \quad (20)$$

where  $\text{SVT}_{b, \beta}(\mathbf{X}) = \mathbf{U} \text{Diag}(\max(\sigma_1 - \beta b_1, 0)), \dots, (\max(\sigma_r - \beta b_r, 0)) \mathbf{V}^T$  denotes the weighted singular value threshold function of  $\mathbf{X}$ ,  $\mathbf{b} = [b_1, b_2, \dots, b_r]$  is the nonnegative



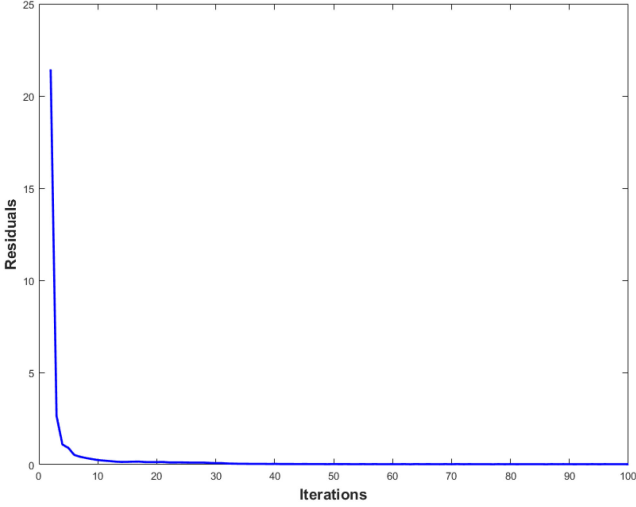


Fig. 1. Residual  $\|\mathbf{G}\mathbf{U}^{(t)} + \mathbf{B}\mathbf{V}^{(t)}\|_F$  as a function of outer loop iteration times for the proposed algorithm.

weighting vector, and the singular value decomposition of  $\mathbf{X}$  is defined by  $\mathbf{X} = \mathbf{U}\mathbf{D}\mathbf{g}(\sigma_1, \dots, \sigma_r)\mathbf{V}^T$ .

The solution of  $\mathbf{V}_4$  is calculated as follows:

$$\begin{aligned} \mathbf{V}_4^{(k+1)} &= \arg \min_{\mathbf{V}_4} \iota_{R^+}(\mathbf{V}_4) + \frac{\mu}{2} \|\mathbf{U}^{(k+1)} - \mathbf{V}_4 - \mathbf{D}_4^{(k)}\|_F^2 \\ &= \max(\mathbf{U}^{(k+1)} - \mathbf{D}_4^{(k)}, 0). \end{aligned} \quad (21)$$

Finally, the Lagrange multipliers are updated as follows:

$$\begin{cases} \mathbf{D}_1^{(k+1)} = \mathbf{D}_1^{(k)} - (\mathbf{A}\mathbf{U}^{(k+1)} - \mathbf{V}_1^{(k+1)}) \\ \mathbf{D}_i^{(k+1)} = \mathbf{D}_i^{(k)} - (\mathbf{U}^{(k+1)} - \mathbf{V}_i^{(k+1)}), i = 2, 3, 4. \end{cases} \quad (22)$$

Summarizing the aforementioned description, we arrive at the complete scheme to solve the SSLRSU model, as presented in Algorithm 1. The proposed SSLRSU algorithm is comprised of inner and outer loop. The outer loop updates the weighting coefficients, and the number of iterations is set to 100. The inner loop updates the Lagrange multipliers in ADMM, and the maximum number of iterations is set to 5. It is difficult to justify the convergence of Algorithm 1. Nevertheless, it is observed that the residual of the original problem generally decreases as the iteration times increase. As shown in Fig. 1, the residual  $\|\mathbf{G}\mathbf{U}^{(t)} + \mathbf{B}\mathbf{V}^{(t)}\|_F$ , as a function of outer loop iteration times for the proposed algorithm, reaches a certain level after only 20 iterations and then levels off. Based on experience, an inner loop with 5 iterations is sufficient to achieve acceptable results in most cases. It can be concluded that the scheme with inner and outer loop not only guarantees the convergence of the algorithm but also accelerates it. When the maximum number of iterations is reached or the residual meets the error tolerance, the proposed algorithm will stop.

### III. EXPERIMENTS WITH SYNTHETIC DATA

In this section, we demonstrate the unmixing performance of the proposed method using two synthetic hyperspectral

---

#### Algorithm 1: Pseudocode of the SSLRSU Algorithm.

---

**1: Initialization:**

2:  $k, t = 0$ , choose  $\mu, \lambda, \tau, \varepsilon > 0$ ,

$\mathbf{U}^{(0)} = (\mathbf{A}^T \mathbf{A} + 3\mathbf{I})^{-1} \mathbf{A}^T \mathbf{Y}$  [45],

$\mathbf{V}_1^{(0)} = \mathbf{A}\mathbf{U}^{(0)}, \mathbf{V}_2^{(0)} = \mathbf{U}^{(0)}, \mathbf{V}_3^{(0)} = \mathbf{U}^{(0)}, \mathbf{V}_4^{(0)} = \mathbf{U}^{(0)}, \mathbf{D}_1^{(0)} = \mathbf{D}_2^{(0)} = \mathbf{D}_3^{(0)} = \mathbf{D}_4^{(0)} = \text{zero}(\text{size}(\mathbf{U}))$

**3: Repeat:**

4:  $\mathbf{H}_1^{(t+1)} \leftarrow$

$$\text{diag} \left[ \frac{1}{\|(\mathbf{U}^{(t)} - \mathbf{D}_2^{(t)})(1,:) \|_2 + \varepsilon}, \dots, \frac{1}{\|(\mathbf{U}^{(t)} - \mathbf{D}_2^{(t)})(m,:) \|_2 + \varepsilon} \right]$$

5:  $\mathbf{H}_{2,ij}^{(t+1)} = \frac{1}{\mathbf{U}_{ij}^{(t)} - \mathbf{D}_{2,ij}^{(t)} + \varepsilon}$

**6: Repeat:**

7:  $\mathbf{U}^{(k+1)} \leftarrow (\mathbf{A}^T \mathbf{A} + 3\mathbf{I})^{-1} (\mathbf{A}^T (\mathbf{V}_1^{(k)} + \mathbf{D}_1^{(k)}) + \mathbf{V}_2^{(k)} + \mathbf{D}_2^{(k)} + \mathbf{V}_3^{(k)} + \mathbf{D}_3^{(k)} + \mathbf{V}_4^{(k)} + \mathbf{D}_4^{(k)})$

8:  $\mathbf{V}_1^{(k+1)} \leftarrow \frac{1}{1+\mu} [\mathbf{Y} + \mu(\mathbf{A}\mathbf{U}^{(k+1)} - \mathbf{D}_1^{(k)})]$

9:  $\mathbf{V}_2^{(k+1)} \leftarrow \text{soft}(\mathbf{U}^{(k+1)} - \mathbf{D}_2^{(k)}, \frac{\lambda}{\mu} \mathbf{H}_1^{(t)} \mathbf{H}_2^{(t)})$

10:  $\mathbf{V}_3^{(k+1)} \leftarrow \text{SVT}_{b, \frac{\tau}{\mu}}(\mathbf{U}^{(k+1)} - \mathbf{D}_3^{(k)})$

11:  $\mathbf{V}_4^{(k+1)} \leftarrow \max(\mathbf{U}^{(k+1)} - \mathbf{D}_4^{(k)}, 0)$

**12: Update Lagrange multipliers:**

13:  $\mathbf{D}_1^{(k+1)} \leftarrow \mathbf{D}_1^{(k)} - \mathbf{A}\mathbf{U}^{(k+1)} + \mathbf{V}_1^{(k+1)}$

14:  $\mathbf{D}_2^{(k+1)} \leftarrow \mathbf{D}_2^{(k)} - \mathbf{U}^{(k+1)} + \mathbf{V}_2^{(k+1)}$

15:  $\mathbf{D}_3^{(k+1)} \leftarrow \mathbf{D}_3^{(k)} - \mathbf{U}^{(k+1)} + \mathbf{V}_3^{(k+1)}$

16:  $\mathbf{D}_4^{(k+1)} \leftarrow \mathbf{D}_4^{(k)} - \mathbf{U}^{(k+1)} + \mathbf{V}_4^{(k+1)}$

17: **Update iteration:**  $k \leftarrow k + 1$

18:  $\mathbf{U}^{(t+1)} \leftarrow \mathbf{U}^{(k)}$

19:  $\mathbf{D}_2^{(t+1)} \leftarrow \mathbf{D}_2^{(k)}$

20: **Update iteration:**  $t \leftarrow t + 1$

21: **Until** some stopping criterion is satisfied.

---

datasets with different characteristics. We compare the proposed SSLRSU algorithm with five advanced sparse unmixing algorithms, including SUnSAL [12], SUnSAL-TV [19], DRSU [16], ADSPRLU [28], and JSpBLRU [31]. The latter three algorithms adopt weighted sparse regression or low-rank constraints.

The signal-to-reconstruction error (SRE, measured in dB) is used to quantitatively evaluate the unmixing accuracy, which is defined as

$$\text{SRE(dB)} = 10 \cdot \log_{10}(E(\|\mathbf{x}\|_2^2)/E(\|\mathbf{x} - \hat{\mathbf{x}}\|_2^2)) \quad (23)$$

where  $\hat{\mathbf{x}}$  denotes the estimated abundance,  $\mathbf{x}$  denotes the true abundance,  $E(\cdot)$  denotes the expectation function.

The probability of success  $p_s$  mentioned in [12] gives an indication about the stability of the estimation. The  $p_s$  is defined as follows:  $p_s \equiv P(\|\hat{\mathbf{x}} - \mathbf{x}\|^2 / \|\mathbf{x}\|^2 \leq \text{threshold})$ . The abundance estimation is considered to be successful when the relative error power of the estimation result is less than a certain threshold, and threshold = 3.16 (5 dB) is demonstrated to be appropriate [12]. The higher SRE(dB) or  $p_s$  value means the better performance of the algorithm. A new indicator called *sparsity* is introduced to measure the proportion of nonzero elements in the estimated abundance [25]. The lower the *sparsity* is, the more sparse the abundance solution is. It should be noted that it is necessary to set

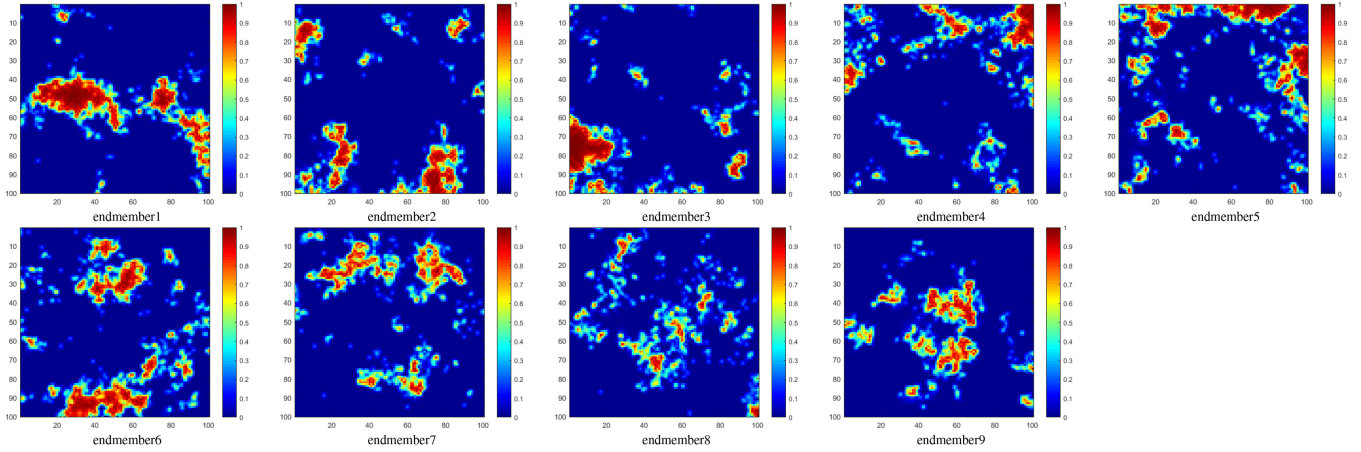


Fig. 2. True fractional abundances of the endmembers in the DC1.

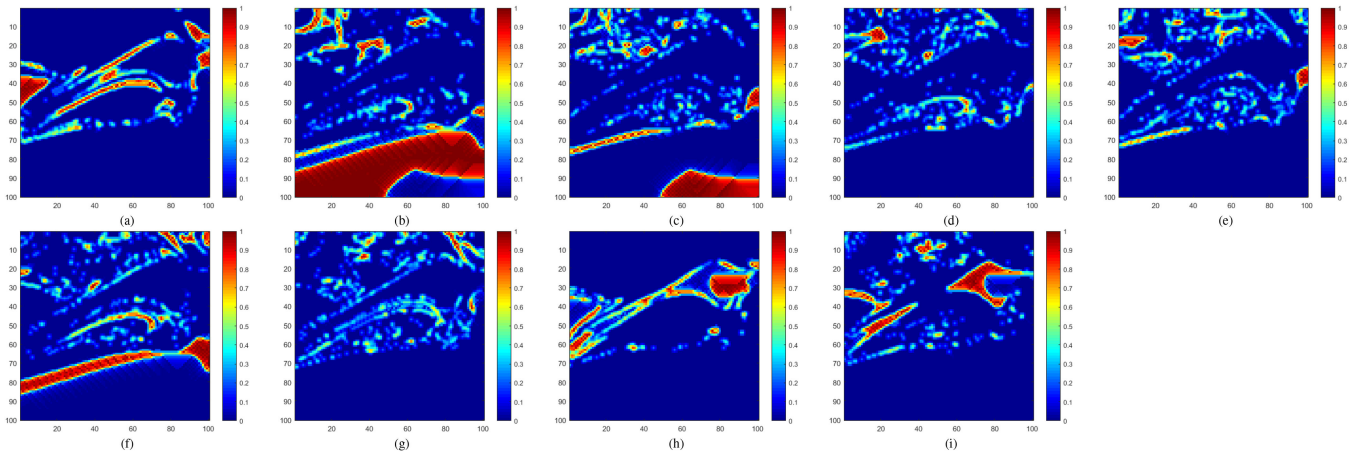


Fig. 3. True fractional abundances of the endmembers in the DC2. (a) Muscovite GDS108 (endmember1). (b) Kaolinite KGa-1. (c) Dumortierite HS190.3B. (d) Nontronite GDS41. (e) Alunite GDS83 Na63. (f) Pyrophyllite PYS1A fine g. (g) Halloysite NMNH106236. (h) Kaolinite CM9. (i) Sphene HS189.3B.

the values in  $\hat{x}$  less than 0.005 to zero via the hard thresholding operation in advance. In all experiments, we tune parameters beforehand for each algorithm and set the maximum number of iterations to 500 to ensure fair competition.

#### A. Simulated Datasets

Two spectral libraries are used in our experiments as minerals dictionaries, which are the subsets of the United States Geological Survey (USGS) library.<sup>1</sup> The spectral library  $\mathbf{A}_1 \in \mathbb{R}^{224 \times 240}$  is comprised of 240 spectral signatures with 224 bands distributed uniformly in the wavelength range of 0.4–2.5  $\mu\text{m}$ . Another spectral library  $\mathbf{A}_2 \in \mathbb{R}^{221 \times 222}$  contains 222 different materials with 221 bands distributed uniformly in the wavelength range of 0.4–2.5  $\mu\text{m}$ . Two simulated data cubes are, respectively, formed by nine endmembers from  $\mathbf{A}_1$  and  $\mathbf{A}_2$  following the linear mixture model. Subsequently, they are contaminated

by white Gaussian i.i.d. noise with three levels of signal-to-noise ratio (SNR): 30, 40, 50 dB. The ANC and ASC are enforced on fractional abundances. The details are explained as follows.

- 1) *Simulated Data Cube 1 (DC1)*: DC1 contains  $100 \times 100$  pixels with 224 bands per pixel. It is generated by nine spectral signatures randomly chosen from the spectral library  $\mathbf{A}_1$ . The fractional abundances with the characteristic of piecewise smooth, also used in [19], reveal the spatial features well for illustrating the relative merits of different algorithms. The true abundance maps of the endmembers are shown in Fig. 2.
- 2) *Simulated Data Cube 2 (DC2)*: DC2 is made up of  $100 \times 100$  pixels with 221 bands. Nine specific endmembers are chosen from  $\mathbf{A}_2$ , as depicted in [46] and [47]. The fractional abundances are created by fractals that imitate the spatial distribution of typical landform in the natural world. The fractional abundance maps associated to each endmember are shown in Fig. 3.

<sup>1</sup>[Online]. Available: <http://speclab.cr.usgs.gov/spectral.lib06>

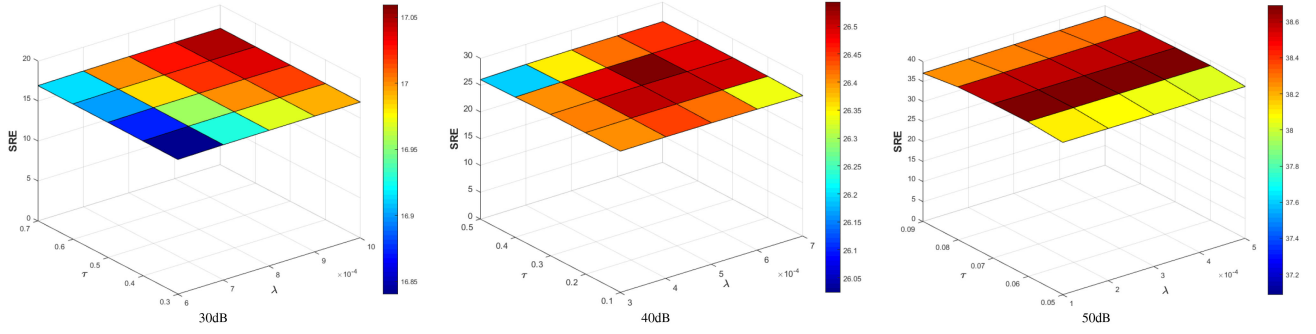


Fig. 4. SRE(dB) as a function of parameters  $\lambda$  and  $\tau$  on DC2 at SNR = 30 dB, 40 dB, 50 dB.

TABLE I

SRE(dB),  $p_s$  AND SPARSITY RESULTS FOR DIFFERENT UNMIXING METHODS ON DC1 (THE OPTIMAL PARAMETER SETTINGS ARE SHOWN IN THE PARENTHESES)

Algorithm	SNR=30dB			SNR=40dB			SNR=50dB		
	SRE(dB)	$p_s$	sparsity	SRE(dB)	$p_s$	sparsity	SRE(dB)	$p_s$	sparsity
SUnSAL	8.4788	0.7970	0.0494	15.0175	0.9866	0.0428	20.7394	1	0.0280
	$(\lambda = 2e-2)$			$(\lambda = 5e-3)$			$(\lambda = 1e-3)$		
SUnSAL-TV	11.3797	0.9457	0.0566	17.7369	0.9998	0.0344	26.0059	1	0.0180
	$(\lambda = 1e-2; \lambda_{TV} = 4e-3)$			$(\lambda = 5e-3; \lambda_{TV} = 1e-3)$			$(\lambda = 2e-3; \lambda_{TV} = 2e-4)$		
DRSU	15.4591	0.9797	0.0246	29.7558	1	0.0138	41.3676	1	0.0119
	$(\lambda = 3e-3)$			$(\lambda = 1e-3)$			$(\lambda = 6e-4)$		
ADSpLRU	16.8309	0.9927	0.0285	29.8436	1	0.0124	40.6707	1	0.0118
	$(\lambda = 2.1; \tau = 8e-4)$			$(\lambda = 1.5; \tau = 2e-4)$			$(\lambda = 3e-1; \tau = 6e-5)$		
JSpBLRU	12.2918	0.9430	0.0289	28.4926	1	0.0155	38.3587	1	0.0126
	$(\lambda = 2; \tau = 4)$			$(\lambda = 8e-1; \tau = 3e-1)$			$(\lambda = 1e-1; \tau = 2e-2)$		
SSLRSU	19.4573	0.9991	0.0157	30.6106	1	0.0124	41.5251	1	0.0119
	$(\lambda = 3e-3; \tau = 1)$			$(\lambda = 2e-3; \tau = 5e-1)$			$(\lambda = 4e-4; \tau = 9e-2)$		

### B. Impact of the Regularization Parameters

There are two regularization parameters  $\lambda$  and  $\tau$  in the proposed method should be concerned, since they are related to the unmixing performance of the algorithm. To analyze the sensitivity of parameters, we take the DC2 at SNR = 30 dB, 40 dB, 50 dB as examples to illustrate the influence of the two parameters in the proposed SSLRSU algorithm. Fig. 4 displays SRE(dB) as a function of parameters  $\lambda$  and  $\tau$ . We can see that surfaces given by the function at different SNR levels are stable around the optimal parameters. That is to say, it is easy to obtain the suboptimal parameters settings, which suggests the robustness of our method. Further analysis shows that the values of optimal parameters  $\lambda$  and  $\tau$  tend to increase with the decrease of SNR. When the noise level is low, the accuracy of the solution is more influenced by the parameter  $\tau$ , and when the noise level is high, the parameter  $\lambda$  plays a more important role.

### C. Results and Discussion

Tables I and II display the mean SRE(dB),  $p_s$ , sparsity results obtained by each algorithm after 50 runs on DC1 and DC2. The optimal parameter settings related to the reported values

are listed in the parentheses. From the tables, we observe that the proposed SSLRSU algorithm achieves the highest SRE(dB) values in all cases, which indicates that joint weighted sparse and low-rank constraints can improve the accuracy of abundance estimation. It is notable that the proposed method shows significant advantage in the case of lower SNR, which verifies its strong antinoise capability. Moreover, compared with other algorithms, the proposed SSLRSU algorithm achieves the larger  $p_s$  values, which proves the stability of abundance estimation. We also see that the SSLRSU and ADSpLRU algorithms generally gain better sparsity than other competitors, which reveals the improvement of the sparsity of the solution by low-rank constraints.

For a visual comparison, Figs. 5 and 6 show the ground-truth abundances and the estimated fractional abundances obtained by different algorithms on DC1 and DC2 at SNR = 30 dB, and only 500 randomly selected pixels are displayed for clarity. Each colored line in figures corresponds to a nonzero vector of the abundance matrix, which represents the proportion of an end-member in images. As seen in Figs. 5 and 6, the abundance maps estimated by the proposed SSLRSU algorithm have the best visual effect, and the abundance lines in the figures are consistent

TABLE II  
SRE(DB),  $p_s$ , AND SPARSITY RESULTS FOR DIFFERENT UNMIXING METHODS ON DC2 (OPTIMAL PARAMETER SETTINGS ARE SHOWN IN THE PARENTHESES)

Algorithm	SNR=30dB			SNR=40dB			SNR=50dB		
	SRE(dB)	$p_s$	sparsity	SRE(dB)	$p_s$	sparsity	SRE(dB)	$p_s$	sparsity
SUnSAL	8.1614	0.7281	0.0571	13.6782	0.9336	0.0507	19.2039	0.9976	0.0317
	$(\lambda = 1e-2)$			$(\lambda = 2e-3)$			$(\lambda = 6e-4)$		
SUnSAL-TV	11.1440	0.8750	0.0673	17.0327	0.9894	0.0459	24.1786	1	0.0241
	$(\lambda = 3e-3; \lambda_{TV} = 3e-3)$			$(\lambda = 6e-4; \lambda_{TV} = 6e-4)$			$(\lambda = 3e-4; \lambda_{TV} = 9e-5)$		
DRSU	13.1418	0.9231	0.0309	26.2944	1	0.0175	38.5275	1	0.0142
	$(\lambda = 1e-3)$			$(\lambda = 5e-4)$			$(\lambda = 3e-4)$		
ADSpLRU	16.6810	0.9733	0.0214	25.1088	0.9998	0.0165	37.6814	1	0.0141
	$(\lambda = 2.4; \tau = 4e-4)$			$(\lambda = 0.7; \tau = 7e-5)$			$(\lambda = 5e-1; \tau = 3e-5)$		
JSpBLRU	15.4816	0.9861	0.0455	25.4461	1	0.0186	35.2931	1	0.0153
	$(\lambda = 6e-1; \tau = 1.3)$			$(\lambda = 4e-1; \tau = 2e-1)$			$(\lambda = 9e-2; \tau = 3e-2)$		
SSLRSU	17.0817	0.9863	0.0205	26.4671	1	0.0164	38.7000	1	0.0142
	$(\lambda = 1e-3; \tau = 6e-1)$			$(\lambda = 5e-4; \tau = 3e-1)$			$(\lambda = 2e-4; \tau = 7e-2)$		

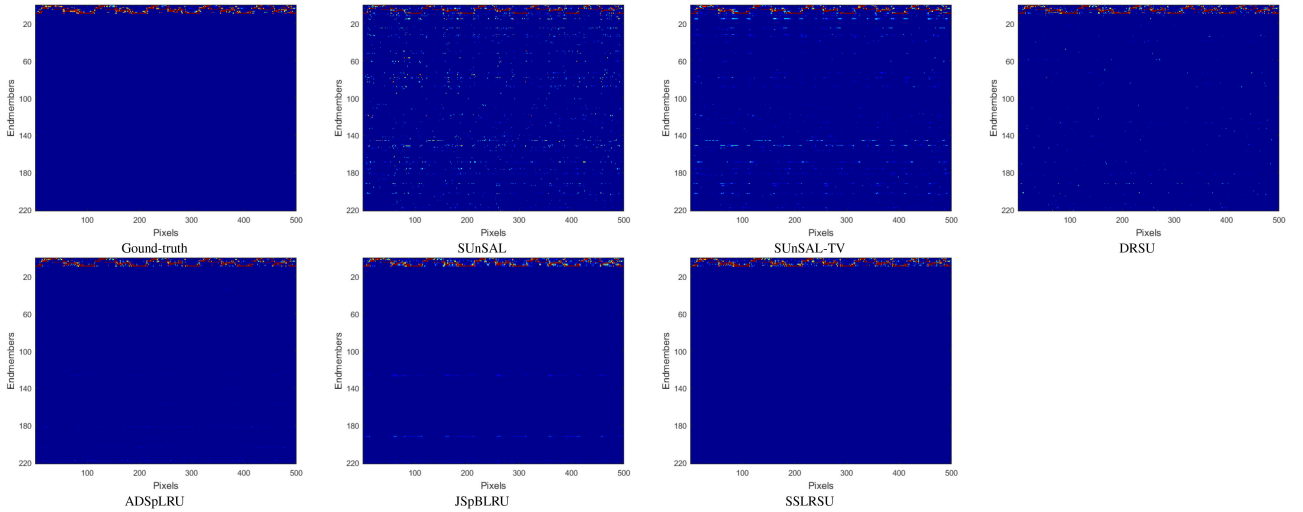


Fig. 5. Ground-truth abundance and the estimated abundances obtained by SUnSAL, SUnSAL-TV, DRSU, ADSpLRU, JSpBLRU and SSLRSU on DC1 when SNR = 30 dB.

with the real ones. Furthermore, the abundance maps obtained by SSLRSU have less noise and fewer outliers, which indicates the advantage of this algorithm in antinoise and endmember identification. Pay attention to the regions where the fractional abundances should be zero, we observe that the abundance maps estimated by the SUnSAL and SUnSAL-TV algorithms contain a lot of noise and false abundance lines. The abundance maps obtained by DRSU are noisy and have several false abundance lines, especially in DC2. Although not as obvious as DRSU, the JSpBLRU algorithm gets a few false endmembers as well. The abundance maps estimated by ADSpLRU are corrupted by interference lines with small values. The abundance maps estimated by the proposed SSLRSU algorithm are closest to the real ones, and there are few false lines in the results. Compared

with algorithms without low-rank constraints (such as DRSU), the combined constraint algorithm shows better performance and concentrates the abundance lines on the primary rows. Compared with the other combined constraint algorithms, the proposed SSLRSU algorithm hardly extracts false endmembers, which indicates that it can achieve accurate matching between the actual spectral signatures in the image and the samples in the spectral library. In other words, the proposed SSLRSU algorithm shows great advantage in identifying endmembers from the spectral library. It is demonstrated that the SSLRSU algorithm effectively avoids the confusing spectral signatures in the library, and partially overcomes the obstacle brought by the high correlation of spectral libraries in sparse unmixing.



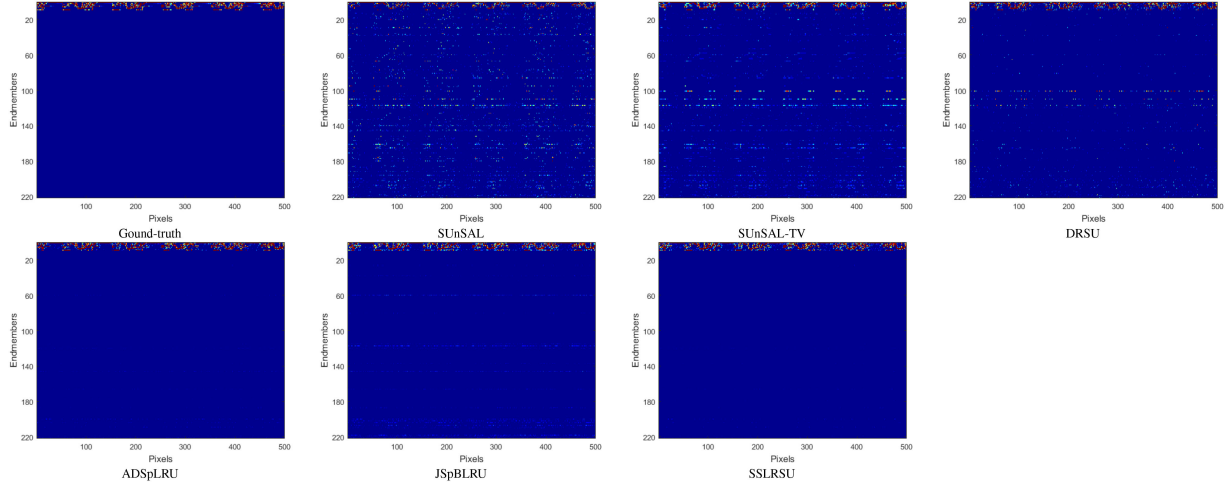


Fig. 6. Ground-truth abundance and the estimated abundances obtained by SUnSAL, SUnSAL-TV, DRSU, ADSpLRU, JSpBLRU, and SSLRSU on DC2 when  $\text{SNR} = 30$  dB.

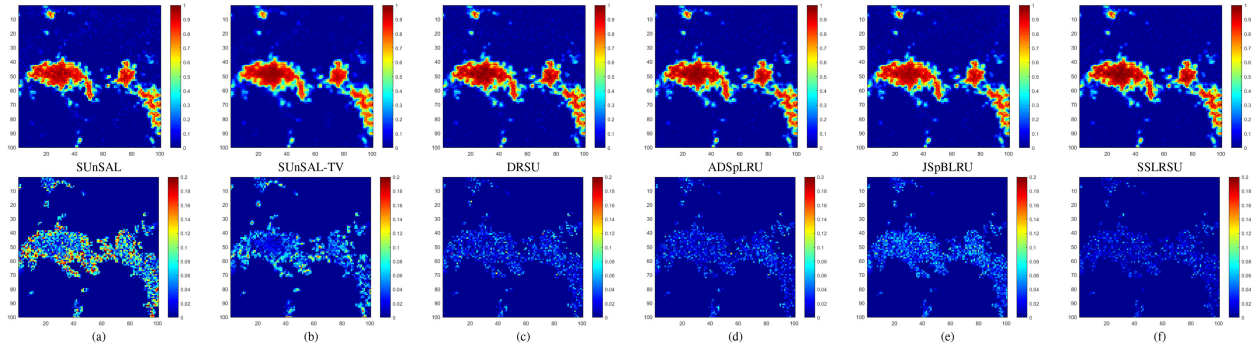


Fig. 7. Fractional abundance maps estimated by SUnSAL, SUnSAL-TV, DRSU, ADSpLRU, JSpBLRU and SSLRSU on DC1 when  $\text{SNR} = 30$  dB. Difference maps between the ground-truth abundance and the results obtained by (a) SUnSAL, (b) SUnSAL-TV, (c) DRSU, (d) ADSpLRU, (e) JSpBLRU, (f) SSLRSU.

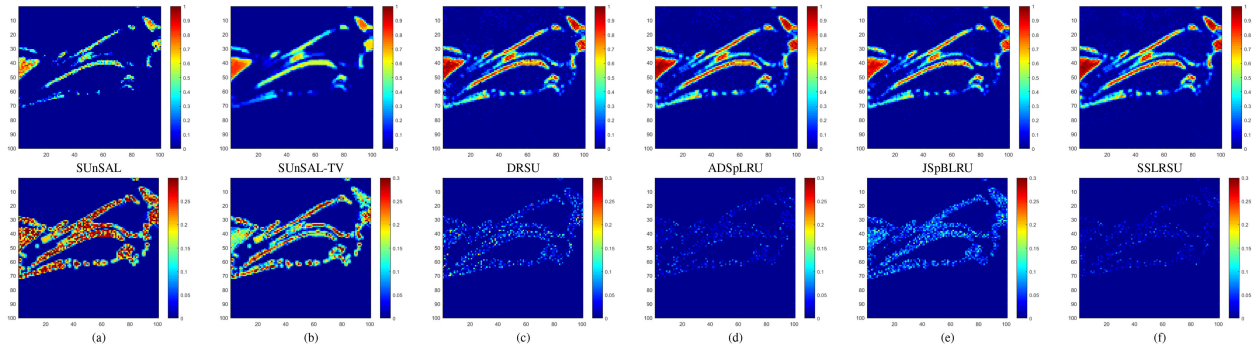


Fig. 8. Fractional abundance maps estimated by SUnSAL, SUnSAL-TV, DRSU, ADSpLRU, JSpBLRU, and SSLRSU on DC2 when  $\text{SNR} = 30$  dB. Difference maps between the ground-truth abundance and the results obtained by (a) SUnSAL, (b) SUnSAL-TV, (c) DRSU, (d) ADSpLRU, (e) JSpBLRU, (f) SSLRSU.

To further illustrate the performance of our SSLRSU algorithm, Figs. 7 and 8 show the fractional abundance maps of each endmember1 in DC1 and DC2 estimated by different methods when  $\text{SNR} = 30$  dB. For intuitive comparison, the figures also show the difference maps between the ground-truth abundances and the estimated abundances. The other endmembers in simulated datasets are elided as they are similar to the exhibited endmembers. From the difference maps, it is found that among all the comparison algorithms, the difference between the

abundance estimated by the proposed SSLRSU algorithm and the true abundance is the smallest, which shows the excellent performance of the proposed method. The results obtained by the SUnSAL algorithm are inaccurate due to the lack of consideration of spatial information. The abundance maps estimated by SUnSAL-TV present blurring and oversmoothing visually. The ADSpLRU and SSLRSU delineate the high fractional abundance regions precisely, while the SSLRSU recovers the details more completely. The superiority of SSLRSU

TABLE III  
COMPUTATIONAL TIMES (IN SECONDS) FOR DIFFERENT UNMIXING METHODS TO PROCESS DC2 WITH AN SNR OF 30 DB

Algorithm	SUnSAL	SUnSAL-TV	DRSU	ADSpLRU	JSpBLRU	SSLRSU
Time(s)	24.75	278.98	75.83	159.98	161.11	164.09

algorithm indicates that the joint of the double weighted sparse regression and the low-rank representation can improve unmixing performance.

Table III reports the processing time for the DC2 with an SNR of 30 dB. All the algorithms are implemented using MATLAB R2016a and tested in the same computing environment: A desktop computer equipped with an Intel Core 7 Duo central processing unit (at 3.6 GHz) and 24 GB of RAM memory. It can be observed that the SSLRSU, ADSpLRU, and JSpBLRU algorithms are faster than SUnSAL-TV. But all of them are slower than SUnSAL and DRSU, due to the increased complexity of the model. Compared with the ADSpLRU and JSpBLRU algorithms that consider low-rank constraints, the proposed SSLRSU algorithm is slightly slower than them, but the calculation time of these three algorithms is roughly the same.

#### IV. EXPERIMENTS WITH REAL DATA

In this section, the notable Airborne Visible Infrared Imaging Spectrometer (AVIRIS) Cuprite scene<sup>2</sup> is embraced for surveying the unmixing execution of the proposed technique. The spatial size of the Cuprite image is  $350 \times 350$ , with 224 spectral bands in the range of  $0.4\text{--}2.5 \mu\text{m}$  and the spectral resolution is 10 nm. Prior to the analysis, due to low SNR and water absorption interference, the bands 1-2105-115, 150-170, and 223-224 were removed. Finally, there are 188 spectral bands left for the experiment. The spectral library  $\mathbf{A}_1 \in \mathbb{R}^{188 \times 240}$  used in the experiment is the same as that used by DC1, and the corresponding noisy bands are also removed. Because it is difficult to obtain the ground-truth abundance of hyperspectral data, the classification map generated by Tricorder 3.3 software product<sup>3</sup> [48] is used as a reference to qualitatively assess the unmixing performance of different methods, as shown in Fig. 9.<sup>4</sup>

Fig. 10 shows the abundance maps estimated by SUnSAL, SUnSAL-TV, DRSU, ADSpLRU, JSpBLRU, and SSLRSU algorithms for three dominant minerals (Alunite, Buddingtonite, and Chalcedony) in Cuprite area. In this experiment, the regularization parameters of SUnSAL and DRSU were empirically set to  $\lambda = 0.001$ ,  $\lambda = 0.0001$ , respectively, whereas the parameters for SUnSAL-TV, ADSpLRU, JSpBLRU, and SSLRSU were set to  $\lambda = 0.001$ ,  $\lambda_{TV} = 0.001$ , and  $\lambda = 0.0005$ ,  $\tau = 0.001$  and  $\lambda = 0.05$ ,  $\tau = 0.2$  and  $\lambda = 0.003$ ,  $\tau = 0.2$ , respectively. It can be seen from Fig. 10 that all the unmixing algorithms can interpret these three minerals well, which indicates that the sparse unmixing algorithm is effective for real hyperspectral datasets. However, we can see that the abundance map (e.g.,

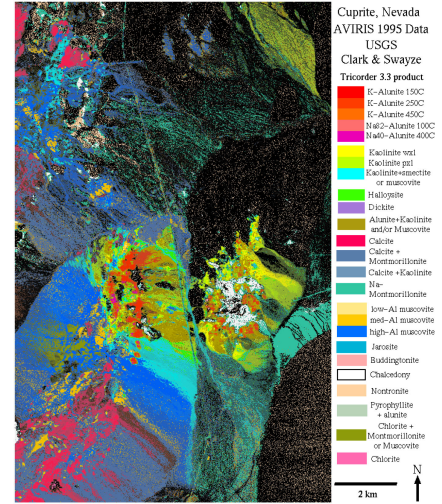


Fig. 9. USGS mineral map of Cuprite mining district in Nevada.

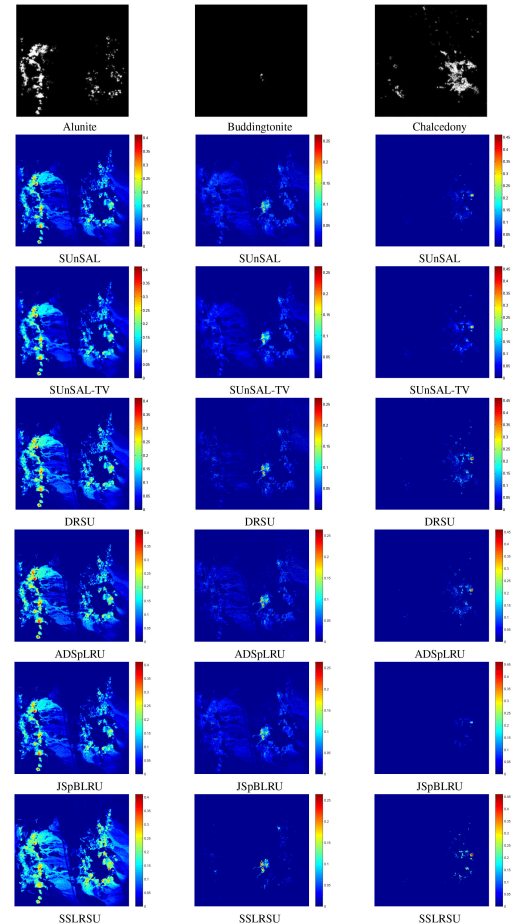


Fig. 10. Fractional abundance maps estimated by SUnSAL, SUnSAL-TV, DRSU, ADSpLRU, JSpBLRU and SSLRSU for the Cuprite subsense.

<sup>2</sup>[Online]. Available: <http://aviris.jpl.nasa.gov/html/aviris.freedata.html>

<sup>3</sup>[Online]. Available: <http://speclab.cr.usgs.gov/PAPER/tetracorder>

<sup>4</sup>[Online]. Available: [http://speclab.cr.usgs.gov/cuprite95.tgif.2.2um\\_map.gif](http://speclab.cr.usgs.gov/cuprite95.tgif.2.2um_map.gif)

Buddingtonite mineral) obtained by the SUnSAL algorithm contain a lot of noise. The abundance maps (e.g., Alunite and Buddingtonite minerals) estimated by the SUnSAL-TV algorithm look oversmoothing. Compared with the DRSU, ADSPRLU, and JSPBLRU algorithms, the abundance maps obtained by the proposed SSLRSU algorithm are closer to the reference map and contain less noise, especially for the Buddingtonite mineral.

In addition, compared with the two algorithms ADSPRLU and JSPBLRU that impose low-rank constraints, the abundance maps estimated by our SSLRSU algorithm are usually comparable or higher in the regions considered as individual materials. Finally, the *sparsity* got by SUnSAL, SUnSAL-TV, DRSU, ADSPRLU, JSPBLRU, and SSLRSU are 0.0682, 0.0743, 0.0430, 0.0471, 0.0728, and 0.0334, respectively. From these small differences, it can be concluded that the proposed method uses fewer elements to interpret the data, thereby obtaining higher sparsity. Therefore, it is concluded from a qualitative point of view that the newly created SSLRSU algorithm exhibits good potential in improving unmixing performance.

## V. CONCLUSION

In this article, a new SSLRSU method has been created for enhanced hyperspectral data analysis. Differing from the previous spectral unmixing algorithms using sparse reduced-rank regression technique, the proposed SSLRSU algorithm traded on the spatial structure characteristics of hyperspectral images, and completely considered the sparsity and linear independence of the row vectors in abundance matrix. The joint constraint strategy improves the ability to identify endmembers from the spectral library, thus effectively alleviating the negative influence of the high mutual interference of the spectral library on the unmixing results. The proposed SSLRSU model is solved iteratively by an inner and outer loop scheme to speed up the convergence of the algorithm. Experimental results with both simulated and real hyperspectral data uncover that the proposed SSLRSU calculation can get steady and precise unmixing results. In future work, we will exploit a tensor-based low-rank representation model [49] for hyperspectral sparse unmixing.

## REFERENCES

- [1] M. Shimoni, R. Haelterman, and C. Perneel, "Hyperspectral imaging for military and security applications: Combining myriad processing and sensing techniques," *IEEE Geosci. Remote Sens. Mag.*, vol. 7, no. 2, pp. 101–117, Jun. 2019.
- [2] S. Li, W. Song, L. Fang, Y. Chen, P. Ghamisi, and J. A. Benediktsson, "Deep learning for hyperspectral image classification: An overview," *IEEE Trans. Geosci. Remote Sens.*, vol. 57, no. 9, pp. 6690–6709, Sep. 2019.
- [3] J. M. Bioucas-Dias, A. Plaza, G. Camps-Valls, P. Scheunders, N. Nasrabadi, and J. Chanussot, "Hyperspectral remote sensing data analysis and future challenges," *IEEE Geosci. Remote Sens. Mag.*, vol. 1, no. 2, pp. 6–36, Jun. 2013.
- [4] J. M. Bioucas-Dias *et al.*, "Hyperspectral unmixing overview: Geometrical, statistical, and sparse regression-based approaches," *IEEE J. Sel. Topics Appl. Earth Observ. Remote Sens.*, vol. 5, no. 2, pp. 354–379, Apr. 2012.
- [5] N. Keshava and J. F. Mustard, "Spectral unmixing," *IEEE Signal Process. Mag.*, vol. 19, no. 1, pp. 44–57, Jan. 2002.
- [6] T. H. Chan, C. Y. Chi, Y. M. Huang, and W. K. Ma, "A convex analysis-based minimum-volume enclosing simplex algorithm for hyperspectral unmixing," *IEEE Trans. Signal Process.*, vol. 57, no. 11, pp. 4418–4432, Nov. 2009.
- [7] J. Li, A. Agathos, D. Zaharie, J. M. Bioucas-Dias, A. Plaza, and X. Li, "Minimum volume simplex analysis: A fast algorithm for linear hyperspectral unmixing," *IEEE Trans. Geosci. Remote Sens.*, vol. 53, no. 9, pp. 5067–5082, Sep. 2015.
- [8] S. Zhang, A. Agathos, and J. Li, "Robust minimum volume simplex analysis for hyperspectral unmixing," *IEEE Trans. Geosci. Remote Sens.*, vol. 55, no. 11, pp. 6431–6439, Nov. 2017.
- [9] L. Miao and H. Qi, "Endmember extraction from highly mixed data using minimum volume constrained nonnegative matrix factorization," *IEEE Trans. Geosci. Remote Sens.*, vol. 45, no. 3, pp. 765–777, Mar. 2007.
- [10] Y. Qian, S. Jia, J. Zhou, and A. Robles-Kelly, "Hyperspectral unmixing via  $l_{1/2}$  sparsity-constrained nonnegative matrix factorization," *IEEE Trans. Geosci. Remote Sens.*, vol. 49, no. 11, pp. 4282–4297, Nov. 2011.
- [11] J. Li, J. M. Bioucas-Dias, A. Plaza, and L. Liu, "Robust collaborative nonnegative matrix factorization for hyperspectral unmixing," *IEEE Trans. Geosci. Remote Sens.*, vol. 54, no. 10, pp. 6076–6090, Oct. 2016.
- [12] M.-D. Iordache, J. M. Bioucas-Dias, and A. Plaza, "Sparse unmixing of hyperspectral data," *IEEE Trans. Geosci. Remote Sens.*, vol. 49, no. 6, pp. 2014–2039, Jun. 2011.
- [13] F. Chen and Y. Zhang, "Sparse hyperspectral unmixing based on constrained  $l_p - l_2$  optimization," *IEEE Geosci. Remote Sens. Lett.*, vol. 10, no. 5, pp. 1142–1146, Sep. 2013.
- [14] X. Xu, Z. Shi, and B. Pan, "L0-based sparse hyperspectral unmixing using spectral information and a multi-objectives formulation," *ISPRS J. Photogramm. Remote Sens.*, vol. 141, pp. 46–58, 2018.
- [15] M.-D. Iordache, J. M. Bioucas-Dias, and A. Plaza, "Collaborative sparse regression for hyperspectral unmixing," *IEEE Trans. Geosci. Remote Sens.*, vol. 52, no. 1, pp. 341–354, Jan. 2014.
- [16] R. Wang, H. C. Li, W. Liao, and A. Pizurica, "Double reweighted sparse regression for hyperspectral unmixing," in *Proc. IEEE Int. Geosci. Remote Sens. Symp.*, Jul. 2016, pp. 6986–6989.
- [17] C. Shi and L. Wang, "Incorporating spatial information in spectral unmixing: A review," *Remote Sens. Environ.*, vol. 149, pp. 70–87, 2014.
- [18] J. Li, Y. Li, R. Song, S. Mei, and Q. Du, "Local spectral similarity preserving regularized robust sparse hyperspectral unmixing," *IEEE Trans. Geosci. Remote Sens.*, vol. 57, no. 10, pp. 7756–7769, Oct. 2019.
- [19] M.-D. Iordache, J. M. Bioucas-Dias, and A. Plaza, "Total variation spatial regularization for sparse hyperspectral unmixing," *IEEE Trans. Geosci. Remote Sens.*, vol. 50, no. 11, pp. 4484–4502, Nov. 2012.
- [20] R. Wang, H. C. Li, A. Pizurica, J. Li, A. Plaza, and W. J. Emery, "Hyperspectral unmixing using double reweighted sparse regression and total variation," *IEEE Geosci. Remote Sens. Lett.*, vol. 14, no. 7, pp. 1146–1150, Jul. 2017.
- [21] H. Li, R. Feng, L. Wang, Y. Zhong, and L. Zhang, "Superpixel-based reweighted low-rank and total variation sparse unmixing for hyperspectral remote sensing imagery," *IEEE Trans. Geosci. Remote Sens.*, vol. 59, no. 1, pp. 629–647, Jan. 2021.
- [22] B. Tu, J. Wang, X. Kang, G. Zhang, X. Ou, and L. Guo, "KNN-based representation of superpixels for hyperspectral image classification," *IEEE J. Sel. Topics Appl. Earth Observ. Remote Sens.*, vol. 11, no. 11, pp. 4032–4047, Nov. 2018.
- [23] X. Xu, J. Li, C. Wu, and A. Plaza, "Regional clustering-based spatial preprocessing for hyperspectral unmixing," *Remote Sens. Environ.*, vol. 204, pp. 333–346, 2018.
- [24] Y. Zhong, R. Feng, and L. Zhang, "Non-local sparse unmixing for hyperspectral remote sensing imagery," *IEEE J. Sel. Topics Appl. Earth Observ. Remote Sens.*, vol. 7, no. 6, pp. 1889–1909, Jun. 2014.
- [25] S. Zhang, J. Li, H. Li, C. Deng, and A. Plaza, "Spectral-spatial weighted sparse regression for hyperspectral image unmixing," *IEEE Trans. Geosci. Remote Sens.*, vol. 56, no. 6, pp. 3265–3276, Jun. 2018.
- [26] Q. Qu, N. M. Nasrabadi, and T. D. Tran, "Abundance estimation for bilinear mixture models via joint sparse and low-rank representation," *IEEE Trans. Geosci. Remote Sens.*, vol. 52, no. 7, pp. 4404–4423, Jul. 2014.
- [27] P. Zheng, H. Su, and Q. Du, "Sparse and low-rank constrained tensor factorization for hyperspectral image unmixing," *IEEE J. Sel. Topics Appl. Earth Observ. Remote Sens.*, vol. 14, pp. 1754–1767, 2021.
- [28] P. V. Giampouras, K. E. Themelis, A. A. Rontogiannis, and K. D. Koutroumbas, "Simultaneously sparse and low-rank abundance matrix estimation for hyperspectral image unmixing," *IEEE Trans. Geosci. Remote Sens.*, vol. 54, no. 8, pp. 4775–4789, Aug. 2016.
- [29] D. Hong and X. X. Zhu, "SULoRA: Subspace unmixing with low-rank attribute embedding for hyperspectral data analysis," *IEEE J. Sel. Topics Signal Process.*, vol. 12, no. 6, pp. 1351–1363, Dec. 2018.



- [30] M. Rizkinia and M. Okuda, "Joint local abundance sparse unmixing for hyperspectral images," *Remote Sens.*, vol. 9, no. 12, pp. 1224, Nov. 2017.
- [31] J. Huang, T. Huang, L. Deng, and X. Zhao, "Joint-sparse-blocks and low-rank representation for hyperspectral unmixing," *IEEE Trans. Geosci. Remote Sens.*, vol. 57, no. 4, pp. 2419–2438, Apr. 2019.
- [32] J. M. Bioucas-Dias and M. Figueiredo, "Alternating direction algorithms for constrained sparse regression: Application to hyperspectral unmixing," in *Proc. IEEE 2nd Workshop Hyperspectral Image Signal Process.-Evol. Remote Sens.*, Jun. 2010, pp. 1–4. doi: [10.1109/WHISPERS.2010.5594963](https://doi.org/10.1109/WHISPERS.2010.5594963).
- [33] E. J. Candès, J. Romberg, and T. Tao, "Stable signal recovery from incomplete and inaccurate measurements," *Commun. Pure Appl. Math.*, vol. 59, no. 8, pp. 1207–1223, Aug. 2006.
- [34] E. J. Candès and T. Tao, "Decoding by linear programming," *IEEE Trans. Inf. Theory*, vol. 51, no. 12, pp. 4203–4215, Dec. 2005.
- [35] M.-D. Iordache, A. Plaza, and J. M. Bioucas-Dias, "On the use of spectral libraries to perform sparse unmixing of hyperspectral data," in *Proc. IEEE Workshop Hyperspectral Image Signal Process.-Evol. Remote Sens.*, 2010, pp. 1–4. doi: [10.1109/WHISPERS.2010.5594888](https://doi.org/10.1109/WHISPERS.2010.5594888).
- [36] A. M. Bruckstein, D. L. Donoho, and M. Elad, "From sparse solutions of systems of equations to sparse modeling of signals and images," *SIAM Rev.*, vol. 51, no. 1, pp. 34–81, 2009.
- [37] P.-A. Thouvenin, N. Dobigeon, and J.-Y. Tournet, "Hyperspectral unmixing with spectral variability using a perturbed linear mixing model," *IEEE Trans. Signal Process.*, vol. 64, no. 2, pp. 525–538, Jan. 2016.
- [38] X. Fu, W. Ma, J. M. Bioucas-Dias, and T. Chan, "Semibind hyperspectral unmixing in the presence of spectral library mismatches," *IEEE Trans. Geosci. Remote Sens.*, vol. 54, no. 9, pp. 5171–5184, Sep. 2016.
- [39] J. Chen and X. Huo, "Theoretical results on sparse representations of multiple-measurement vectors," *IEEE Trans. Signal Process.*, vol. 54, no. 12, pp. 4634–4643, Dec. 2006.
- [40] C. Y. Zheng, H. Li, Q. Wang, and C. L. Philip Chen, "Reweighted sparse regression for hyperspectral unmixing," *IEEE Trans. Geosci. Remote Sens.*, vol. 54, no. 1, pp. 479–488, Jan. 2016.
- [41] M. Fazel, T. K. Pong, D. Sun, and P. Tseng, "Hankel matrix rank minimization with applications to system identification and realization," *SIAM J. Matrix Anal. Appl.*, vol. 34, no. 3, pp. 946–977, Jul. 2013.
- [42] Z. Hu, F. Nie, R. Wang, and X. Li, "Low rank regularization: A review," *Neural Netw.*, vol. 136, pp. 218–232, Apr. 2021.
- [43] S. Gu, L. Zhang, W. Zuo, and X. Feng, "Weighted nuclear norm minimization with application to image denoising," in *Proc. IEEE Conf. Comput. Vis. Pattern Recog.*, Jun. 2014, pp. 2862–2869.
- [44] Z. Lin, "A review on low-rank models in data analysis," *Big Data Inf. Analytics*, vol. 1, no. 2/3, p. 139, 2016.
- [45] A. N. Tikhonov, "Solution of incorrectly formulated problem and the regularization method," *Sov. Math. Dokl.*, vol. 4, pp. 1036–1038, 1963.
- [46] G. Martin and A. Plaza, "Region-based spatial preprocessing for endmember extraction and spectral unmixing," *IEEE Geosci. Remote Sens. Lett.*, vol. 8, no. 4, pp. 745–749, Jul. 2011.
- [47] G. Martin and A. Plaza, "Spatial-spectral preprocessing prior to endmember identification and unmixing of remotely sensed hyperspectral data," *IEEE J. Sel. Topics Appl. Earth Observ. Remote Sens.*, vol. 5, no. 2, pp. 380–395, Apr. 2012.
- [48] R. Clark *et al.*, "Imaging spectroscopy: Earth and planetary remote sensing with the USGS tetracorder and expert systems," *J. Geophys. Res.*, vol. 108, no. E12, pp. 5131–5135, Dec. 2003.
- [49] L. Sun, F. Wu, T. Zhan, W. Liu, J. Wang, and B. Jeon, "Weighted nonlocal low-rank tensor decomposition method for sparse unmixing of hyperspectral images," *IEEE J. Sel. Topics Appl. Earth Observ. Remote Sens.*, vol. 13, pp. 1174–1188, 2020.



**Fan Li** received the B.S. degree in computer science and technology from Wuhan University, Wuhan, China, in 2004, and the M.E. degree in computer technology from Jiangxi Normal University, Nanchang, China, in 2020.

She is currently a Lecturer with the School of Information Engineering, Nanchang Institute of Technology, Nanchang, China. Her research interests include hyperspectral unmixing, low-rank representation.



machine learning.



**Shaoquan Zhang** (Member, IEEE) received the B.S. degree in communication engineering and the M.E. degree in power engineering from Nanchang Institute of Technology, Nanchang, China, in 2012 and 2015, respectively, and the Ph.D. degree in cartography and geography information system from Sun Yat-sen University, Guangzhou, China, in 2018.

He is currently a lecturer with the School of Information Engineering, Nanchang Institute of Technology, Nanchang, China. His research interests include hyperspectral unmixing, sparse representation, and

**Bingkun Liang** received the B.S. degree in civil engineering from Hunan Agricultural University, Changsha, China, in 2016, and the M.S. degree in ethnology from Sun Yat-Sen University, Guangzhou, China, in 2019.

He is currently pursuing the Ph.D. degree in cartography and geography information system with the School of Geography and Planning, Sun Yat-sen University, Guangzhou, China. His major research interests include spectral unmixing, signal processing, and remote sensing.



**Chengzhi Deng** received the B.S. degree in communication engineering and the M.S. degree in optics from Jiangxi Normal University, Nanchang, China, in 2002 and 2005, and the Ph.D. degree in information and communication engineering from the Huazhong University of Science and Technology, Wuhan, China, in 2008.

He is currently a professor with the School of Information Engineering, Nanchang Institute of Technology, Nanchang, China. He is also the Deputy Director of Jiangxi Province Key Laboratory of Water Information Cooperative Sensing and Intelligent Processing. His research interests include hyperspectral image processing, machine learning, and remote sensing of water environment.



**Chenguang Xu** received the B.S. degree in communication engineering from the East China University of Technology, Fuzhou, China, in 2007, and the M.E. degree in power engineering from the Nanchang Institute of Technology, Nanchang, China, in 2017.

He is currently a lecturer with the School of Information Engineering, Nanchang Institute of Technology, Nanchang, China. His major research interests include hyperspectral unmixing and sparse representation.



**Shengqian Wang** received the M.S. degree in theoretical physics from Jiangxi Normal University, Nanchang, China, in 1995, and the Ph.D. degree in information and communication engineering from Shanghai Jiao Tong University, Shanghai, China, in 2002. He is currently a professor with the School of Information Engineering, Nanchang Institute of Technology, Nanchang, China.

He is also the Director of Jiangxi Province Key Laboratory of Water Information Cooperative Sensing and Intelligent Processing. His research interests include hyperspectral image processing, machine learning, and hydrological information processing.